Materials Today Communications 31 (2022) 103531

Contents lists available at ScienceDirect

Materials Today Communications

journal homepage: www.elsevier.com/locate/mtcomm

The effect of Ni or Co additions on the structure of $Zr_{60}Cu_{30}Al_{10}$ bulk metallic glass revealed by high-energy synchrotron radiation

Martin E. Stiehler [a,*], Nikolaos T. Panagiotopoulos [b], Dean S. Keeble [c], Yurii P. Ivanov [b], Melita Menelaou [d], Mark R. Jolly [a], A. Lindsay Greer [b], Konstantinos Georgarakis [a]

[a] School of Aerospace, Transport and Manufacturing, Cranfield University, Cranfield MK43 0AL, UK
[b] Department of Materials Science & Metallurgy, University of Cambridge, Cambridge CB3 0FS, UK
[c] Diamond Light Source Ltd., Didcot OX11 0DE, UK
[d] Cyprus University of Technology, 3603 Limassol, Cyprus

ARTICLE INFO

Keywords:
Metallic glass
Atomic structure
Pair distribution function
Glass forming ability
X-ray diffraction
Synchrotron radiation
Disorder
Confusion principle
Anti-shell
Emergence
TEM
DSC

ABSTRACT

The effect of substituting Cu by elemental additions of Ni or Co on the atomic structure of the $Zr_{60}Cu_{30}Al_{10}$ ternary bulk metallic glass (BMG) is studied using high-energy synchrotron radiation X-ray diffraction. Analyses of the structural features in reciprocal and real space using the structure factors $S(Q)$ and pair-distribution functions (PDF) point to an increase in the structural disorder for the Ni- or Co-bearing quaternary alloys. This is consistent with the "confusion principle" since upon alloying the initially nearly identical atomic sizes of Cu, Ni and Co diversify due to local electronic interactions. In real space, the disordering is manifested by a reduced deviation from the average particle density visible in the nearest-neighbour (NN) atomic shell structure over the complete short- and medium-range order region. Despite their similar atomic size, enthalpies of mixing with the main alloy elements and apparent disordering of the structure, the additions of Ni or Co have different effects on thermal stability of the ternary "mother" alloy.

1. Introduction

Due to their amorphous structure, bulk metallic glasses (BMGs) exhibit interesting engineering properties typically superior to those of their conventional crystalline counterparts [1–5]. However, glass formation in metallic alloys is still not well understood. A variety of parameters and rules have been considered for the prediction and enhancement of their glass-forming ability (GFA). Amongst them are the "confusion principle" suggesting that a mixture of many elements with a high diversity especially in the atomic radii could lead to dense packing in the liquid state favouring glass formation over crystallisation upon rapid solidification [6,7] and Inoue's three empirical rules [8]. The latter state that enhanced GFA can often be found (i) in alloys with more than three components, (ii) when the three main components exhibit significantly different atomic sizes (differences $\gtrapprox$12%) and (iii) when enthalpies of mixing ΔH_{mix} between the three main components are negative. In a sense, the first and second of Inoue's rules specify different routes that can be taken to effectively "confuse" the liquid alloy's structure to avoid crystallisation by increasing the diversity in the properties among the components present, particularly their different sizes [7]. Further factors that influence GFA are, inter alia, the crystal-liquid interfacial free energy [9–11], the diffusivity of the components [12,13] as well as the alloy's proximity to eutectic compositions [10,14] or triple points [10,15] in their phase diagrams. The existence of eutectics and triple points themselves can be considered to arise from a kind of "structural confusion" due to competing orderings (e.g. different crystalline phases) [10,16–18]. Comparably, the dissimilarities of short- (SRO) and medium-range order (MRO) of the undercooled liquid phase and competing crystalline phases are another source of "confusion" that may be beneficial for GFA [10,17,19]. However, a rigorous way of quantifying "confusion" and disorder from a structural point of view is missing so far, and exceptions to virtually all of the aforementioned rules – towards lower as well as higher GFA – exist [20–25]. Ultimately, the necessary prerequisites for high GFA have to be explained by the interplay of the electrons and atoms in a material. Those electronic interactions can be discussed in a local [26] as well as a global view

* Corresponding author.
E-mail address: martin.stiehler@cranfield.ac.uk (M.E. Stiehler).

https://doi.org/10.1016/j.mtcomm.2022.103531
Received 27 February 2021; Received in revised form 1 April 2022; Accepted 10 April 2022
Available online 13 April 2022
2352-4928/© 2022 The Author(s). Published by Elsevier Ltd. This is an open access article under the CC BY license (http://creativecommons.org/licenses/by/4.0/).

[27–29].

Using high-energy X-ray diffraction (XRD) and pair-distribution function (PDF) analysis the effect of Al addition on SRO and MRO of the amorphous structure in Zr-Cu-Al BMGs in relation to their GFA and other properties has previously been shown [30–32]. While the structure of binary Zr-Cu metallic glasses can be approximated by models equivalent to an ideal-solution-like behaviour [33], addition of Al strongly modifies the atomic structure leading to the formation of Zr-Al nearest-neighbour (NN) populations far in excess of the random statistics of an ideal solution model [30]. In this respect, the structure of the hypoeutectic ternary alloy $Zr_{60}Cu_{30}Al_{10}$ has recently been studied by different techniques [31,32]. Using high-energy synchrotron radiation combined with containerless levitation the structural changes in this alloy were continuously probed during in-situ vitrification, starting from the high-temperature liquid down to the amorphous solid. The findings suggested that the addition of Al introduces strong covalent-like bonding resulting in stronger cohesion and increased population of local polyhedral atomic clusters, i.e. enhancing their stability through local electronic interactions associated with bond shortening [34] which in turn is responsible for sluggish kinetics in the undercooled liquid favouring vitrification.

Additions of Ni are known to significantly increase GFA and thermal stability of Zr-Cu-Al alloys, achieving a critical diameter d_c (i.e. the maximum diameter of a sample that can be cast fully glassy) of up to 30 mm [37–39]. Additions of Co, on the other hand, have a smaller effect on GFA with maximum reported d_c values for the Zr-Cu-Co-Al system of 12 mm [40]. At first glance, the increase in the number of components in going from the ternary Zr-Cu-Al to the quaternary Zr-Cu-TM-Al (with TM being either Ni or Co) systems could be responsible for the increased GFA due to an increase of diversity and confusion in the alloys. However, the atomic sizes of Cu, Ni and Co are so close to each other (Fig. 1) that identical bond lengths d_{at} with Zr and Al have to be assumed [41]. This would (neglecting further effects like the proximity to eutectic compositions) remove the second and to some extent also the first route of increasing confusion according to Inoue's rules and no change of GFA should take place. Inoue's third empirical rule, however, could still provide the possibility of an enhanced GFA since the addition of Ni or Co introduces elemental pairs with considerably higher negative values of ΔH_{mix} compared to those in the ternary alloy (Fig. 1, bold). Related to that, another source of diversity may arise from the different electronic configuration of Ni or Co compared to that of Cu. While, at least for the free atoms, all 3d states of Cu are filled, Ni and Co possess one and two unoccupied 3d states, respectively. Based on this, changes of the chemical bonding network of $Zr_{60}Cu_{30}Al_{10}$ with addition of Ni or Co can be expected.

In the present work the atomic structure of the ternary alloy $Zr_{60}Cu_{30}Al_{10}$ as well as the quaternary alloys $Zr_{60}Cu_{20}Ni_{10}Al_{10}$ and $Zr_{60}Cu_{20}Co_{10}Al_{10}$ were studied using high energy synchrotron radiation X-ray diffraction. Despite the very similar properties of Cu, Ni and Co, characteristic structural changes induced by the addition of Ni or Co to $Zr_{60}Cu_{30}Al_{10}$ could be identified. The associated effects on thermal stability of the glassy alloys are discussed.

2. Materials and methods

2.1. Sample preparation and characterisation

Samples of three alloys with nominal compositions (in at%) $Zr_{60}Cu_{30}Al_{10}$, $Zr_{60}Cu_{20}Ni_{10}Al_{10}$ and $Zr_{60}Cu_{20}Co_{10}Al_{10}$ were prepared by arc-melting from high-purity raw materials (Zr: 99.5%, Co: 99.9%, Ni: 99.9%, Cu: 99.9%, Al: 99.9%) under Ar atmosphere. The ingots were flipped and re-melted four times as well as electromagnetically stirred during each step. Subsequent suction-casting of the ingots into a water-cooled Cu-mould was employed to obtain cylindrical samples 1 mm in diameter.

An FEI Osiris transmission electron microscope (TEM) equipped with a high-brightness field-emission gun was used to obtain high-resolution images indicating the amorphous nature of the samples. Additionally, high-angle annular dark-field (HAADF) imaging and energy-dispersive X-ray (EDX) spectroscopy was carried out to investigate the distribution of the alloying elements in the samples.

Differential scanning calorimetry (DSC) was employed to determine characteristic temperatures and to evaluate the thermal stability of the glassy alloys. A TA Instruments Q2000 DSC was used to measure the glass-transition temperatures T_g and the crystallisation temperatures T_X. Alloy samples with masses of about 10 mg were encased in Al pans with lids. During a first heating run the samples were heated up to 823 K, i.e. well above T_X. After cooling down to room temperature, the same protocol was used on the crystallised samples to obtain the baselines. A TA Instruments Q600 DSC/TGA was used to identify the liquidus temperatures T_l. Samples with masses of about 9 mg were placed in Al_2O_3 pans without lids. All heating runs were performed at a heating rate of 0.667 K/s.

High-energy X-ray diffraction experiments in transmission mode were carried out at beamline I15-1 of the Diamond Light Source using an incident monochromatic beam with a wavelength of $\lambda_i = 0.161669$ Å ($E_i = 76.69$ keV). A Perkin Elmer XRD 4343 CT flat-panel detector was used for the acquisition of diffraction data up to a maximum momentum transfer of 38.86 $Å^{-1}$. LaB_6 was used to calibrate the scattering geometry. A beam spot size of 10 × 700 μm^2 and an acquisition time of 600 s per sample were used. This enabled the collection of diffraction data with sufficient statistics for very high signal-to-noise ratio and reliable PDFs. The diffraction images, after necessary corrections for polarisation, dark current and air (background) scattering, were azimuthally

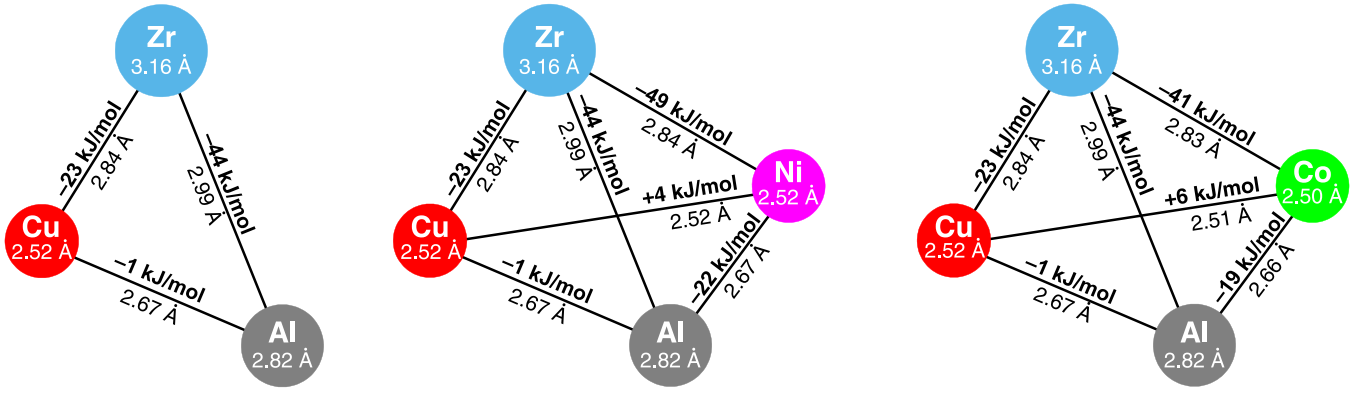

Fig. 1. Enthalpies of mixing ΔH_{mix} (bold) according to Miedema's model [35] and interatomic distances d_{at} [36] for all pairs of elements in the three alloys under consideration. The interatomic distance for pairs of the same element equals the atomic diameter of this element [36] and is noted at each element. The numerical values can also be found in Table S1 in the Supplementary Material.

integrated using the DAWN software [42,43]. From the so-obtained integrated diffraction intensities $I(Q)$ the total structure factors $S(Q)$ where calculated using the GudrunX software [44] following corrections for absorption, fluorescence, Compton scattering, background contribution as well as normalisation to the X-ray atomic form factor and conversion to electron units per atom with the generalised Krogh-Moe-Norman method [45,46]. GudrunX was also used to Fourier transform $S(Q)$ [47] to the reduced pair-distribution function

$$G(r) = \frac{2}{\pi}\int_0^{Q_{max}} Q[S(Q) - 1]\sin(Qr)\mathrm{d}Q = 4\pi r[\rho(r) - \rho_0] \quad (1)$$

to obtain structural information in real space, where r is the radial distance from a centre atom, ρ_0 the average particle number density and $\rho(r)$ represents the local atomic-pair density (atomic-pair density function) [47]. While ideally Q_{max} in Eq. (1) is infinite, in practice it is necessary to choose a finite value as high as possible, depending on the raw data. In the present study a value of $Q_{max} = 25$ Å^{-1} was used.

2.2. Nearest-neighbour shells and the concept of "anti-shells"

The pair-distribution function is a useful tool for analysing the atomic structure in amorphous systems [48]. Fig. 2 shows schematically the reduced pair-distribution function $G(r)$ of a metallic amorphous material. The broad peaks (or maxima) in the $G(r)$ functions correspond to the NN coordination shells with locally higher density of atoms. The valleys (minima) in $G(r)$ correspond to positions (r-distances) with lower local density of atoms; they are often thought of as the edges of the coordination shells. However, there is no unique definition of the cut-off distance that signifies where one shell ends and the next one begins. This ambiguity in some cases complicates discussion of the trends observed in these minima. Thus, the concept of "anti-shells" is introduced here as a tool to facilitate this discussion and complement the definition of the NN shells. For the $G(r)$ functions, areas with values $G(r) < 0$ can be considered as "anti-shells" (areas hatched orange in Fig. 2a), whereas areas where $G(r) > 0$ correspond to the NN shells (areas shown green in Fig. 2). For other expressions of the pair correlations, the definitions should be modified accordingly; for example for $g(r)$ (pair-distribution function [47]) which oscillates around $g(r) = 1$, the shells would be found in areas with $g(r) > 1$ and the anti-shells for $g(r) < 1$. It is envisaged that the shell/anti-shell concept would allow for a more rigorous, less subjective and more reliable way of determining structural metrics (e.g. area, height or centre of mass of a peak) by using a reference inherently associated with the structure function itself (e.g. $G(r) = 0$ in the case of the reduced pair-distribution function) without the need for any background subtraction or fitting procedure.

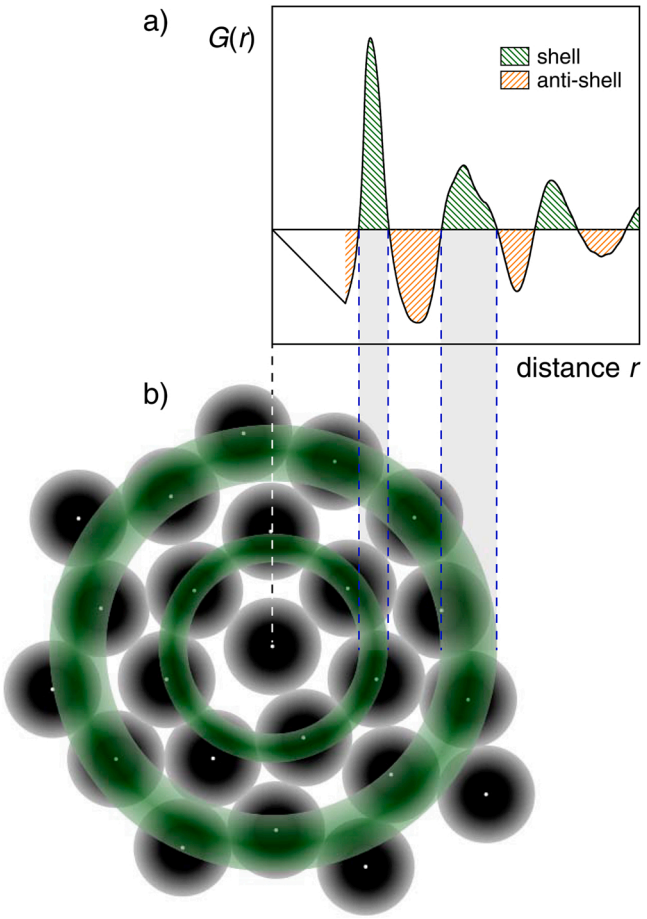

Fig. 2. Schematic representation of the reduced pair distribution function $G(r)$ to illustrate the definition of NN shells and anti-shells (a) and their relation to the atomic arrangement in a two-dimensional monatomic model glass (b). The centres of the atoms in (b) are marked by white dots. The areas of the atoms shaded in grey symbolise the softness of the interatomic potential.

3. Results

Fig. 3 shows high-resolution transmission electron microscopy (HRTEM) images of the three alloys $Zr_{60}Cu_{30}Al_{10}$, $Zr_{60}Cu_{20}Ni_{10}Al_{10}$ and $Zr_{60}Cu_{20}Co_{10}Al_{10}$. The HRTEM images show homogeneous amorphous structures for the three alloys, without any presence of lattice fringes. The HAADF images and EDX mappings in Fig. 4 further confirm the homogeneous amorphous structure of these samples, without any indications of phase separation or other structural inhomogeneity at this scale. Phase separation has been reported in glassy $Zr_{60}Cu_{20}Co_{10}Al_{10}$ after annealing by Wang et al. [49]. In the present work, however, the HRTEM and HAADF observations (Figs. 3 and 4) rule out phase separation in the as-cast samples.

Fig. 5a shows the structure factors $S(Q)$ for $Zr_{60}Cu_{30}Al_{10}$, $Zr_{60}Cu_{20}Ni_{10}Al_{10}$ and $Zr_{60}Cu_{20}Co_{10}Al_{10}$ up to 18 Å^{-1}. The three alloys exhibit very similar structure factors with diffuse peaks typical for amorphous alloys and decaying intensity with increasing Q. No Bragg peaks could be observed up to the maximal Q of 38.86 Å^{-1}. For the remainder of this paper these diffuse peaks in reciprocal space will be referred to as halos which are numbered as shown in Fig. 5a. Starting from the features of $S(Q)$ for the ternary $Zr_{60}Cu_{30}Al_{10}$ alloy, the subtle differences induced by the addition of Ni and Co are discussed. The first halo, which bears information mainly from the MRO in real space [50,51], is very distinct and almost symmetrical. Interestingly, the addition of Ni or Co leads to a decrease of its intensity while its position ($Q_1 = 2.59$ Å^{-1}) and width remain virtually unchanged (Fig. 5a). Taking into account the very similar X-ray form factors of Cu, Ni and Co, this observation may be related to an increase in the structural disorder caused by Ni or Co addition, without significant change of the principal structure. While the changes in going from the ternary to the quaternary alloys are distinct, the difference between the two quaternary alloys is relatively small. The second halo shows a structure consisting of (at least) two features that are frequently observed in metallic glasses [52]. These two features, denoted as 2 l (at the *l*ow-Q side) and 2 h (at the *h*igh-Q side) are not separated by a local minimum, i.e. feature 2 h remains a shoulder for all three alloys leaving halo 2 with a skewness towards higher Q. The split of the second halo has previously been discussed in connection with icosahedral SRO which is assumed to be the prevailing motif in Zr-based BMGs and critical for their high GFA [53–56]. Experimentally, as well as by simulations, icosahedral order has been shown to dominate the SRO in $Zr_{60}Cu_{30}Al_{10}$ [32]. It is interesting to note that the intensity of sub-halo 2 h stays virtually unaffected whereas the intensity of 2 l changes (decreases) markedly (Fig. 5). In other Zr-bearing metallic glasses an increasing intensity of the low-Q feature was related to increasing ordering [57], indicating again an increasing disorder by alloying with Ni or Co in the present case.

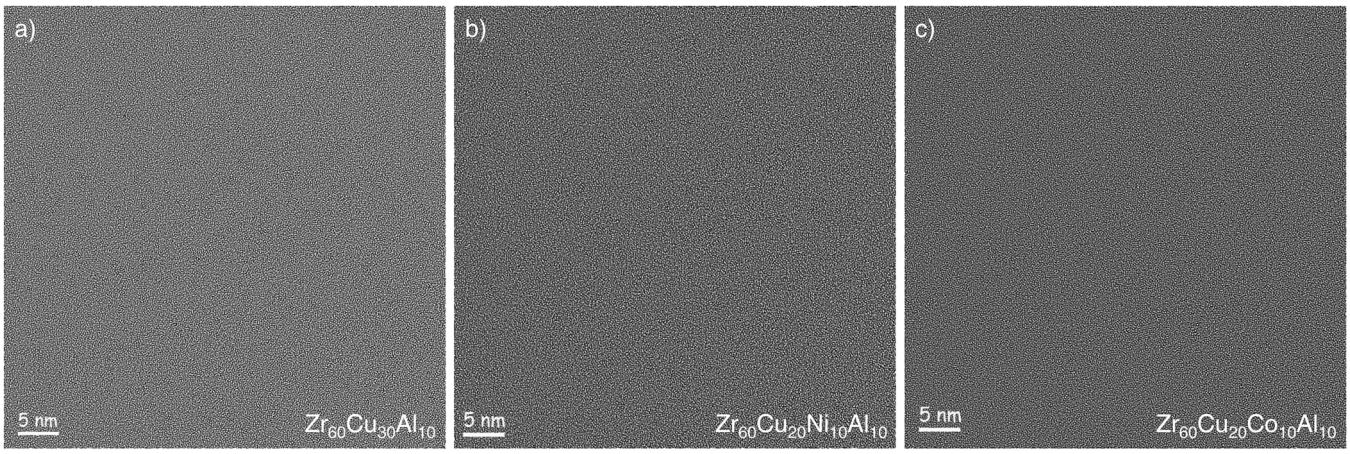

Fig. 3. Transmission electron micrographs for the three alloys $Zr_{60}Cu_{30}Al_{10}$, $Zr_{60}Cu_{20}Ni_{10}Al_{10}$ and $Zr_{60}Cu_{20}Co_{10}Al_{10}$ corroborating their homogeneous amorphous structure.

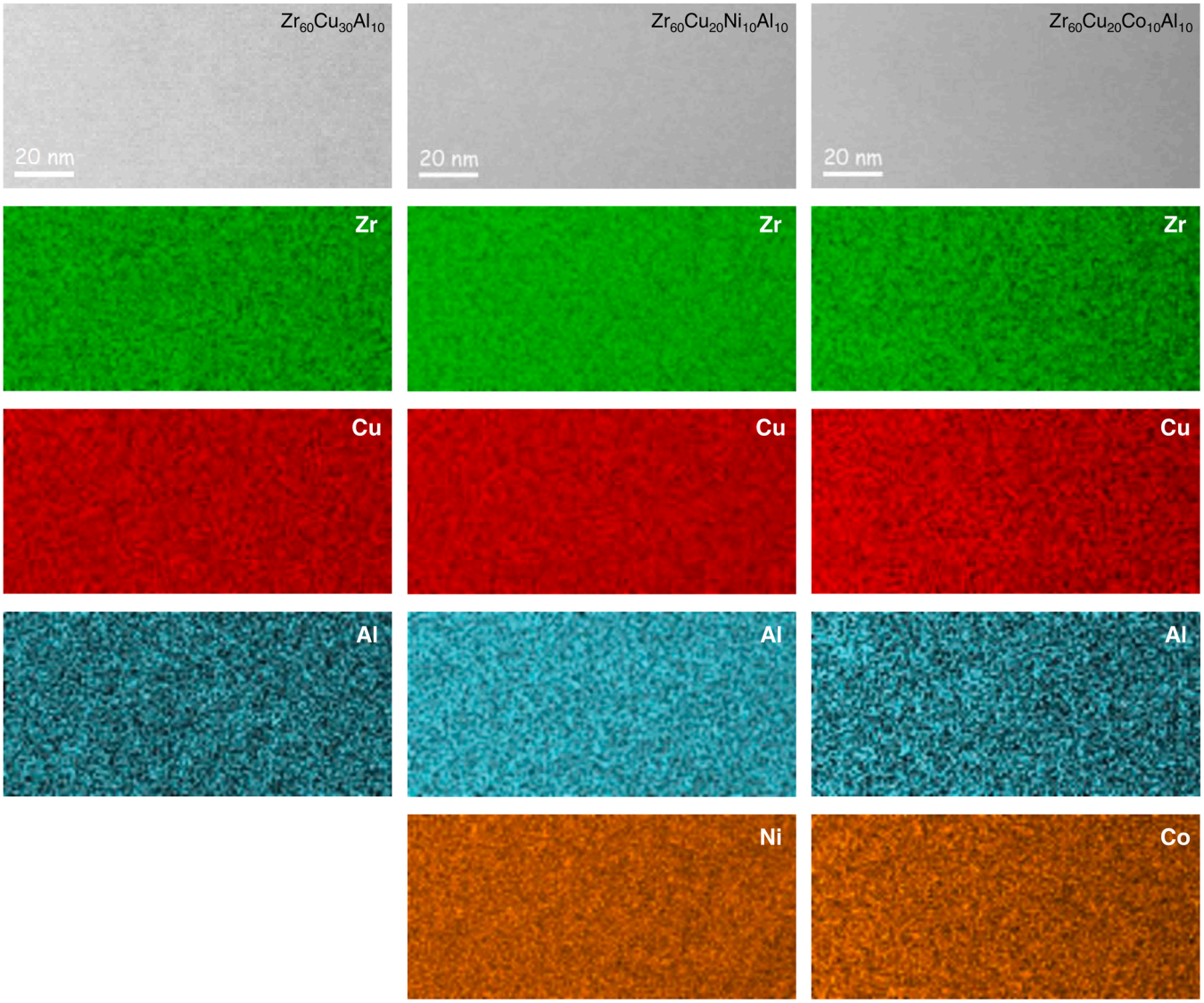

Fig. 4. HAADF images (top) and EDX mappings for the individual elements in the three samples highlighting their compositional homogeneity.

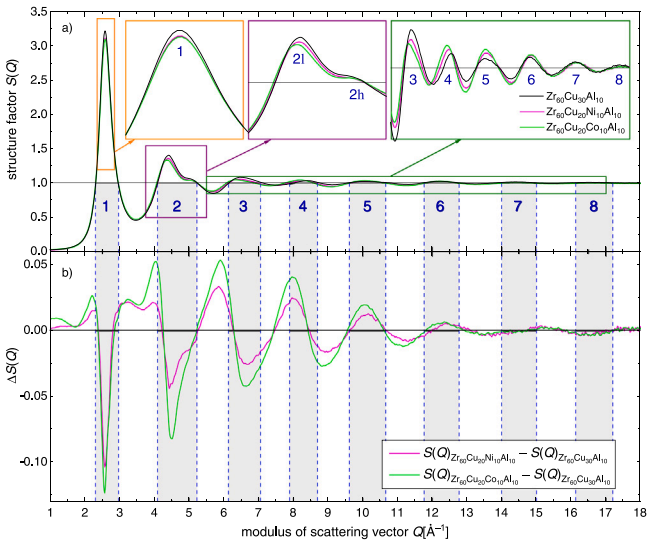

Fig. 5. a) Structure factors $S(Q)$ up to 18 Å^{-1} of all three alloys together with several enlarged views for the first 8 halos (as numbered) and b) the difference functions $\Delta S(Q)$ with respect to $S(Q)$ of $Zr_{60}Cu_{30}Al_{10}$. The vertical dotted lines and the shaded areas highlight the Q-ranges of the halos.

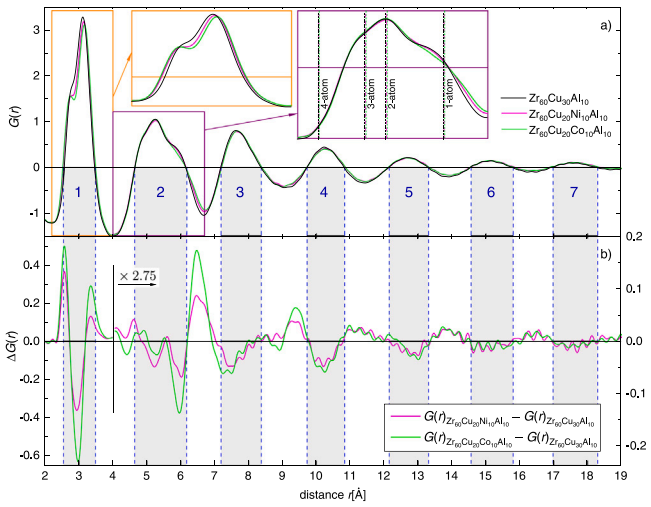

Fig. 6. a) The reduced pair distribution functions $G(r)$ for all three alloys together with enlarged views for the first and second NN shell. The dotted vertical lines and shaded areas highlight the regions of the NN shells (as numbered). Vertical lines in the inset for the second NN shell mark expected distances if interconnected coordination polyhedra sharing 1-, 2-, 3- and 4-atoms, respectively, are assumed. b) Differences $\Delta G(r)$ in the reduced PDF induced by alloying (the y-axis has been scaled by a factor of 2.75 from $r = 4$ Å onwards for clarity).

The trend of decreasing intensity of $S(Q)$ with Ni or Co addition can be observed up to the third halo (Fig. 5a). For the higher-order halos (right inset of Fig. 5a) this sequence is reversed, with the intensity of halos 4–6 for the Ni- and Co-bearing alloys becoming higher than those of $Zr_{60}Cu_{30}Al_{10}$. This and some other peculiarities of $S(Q)$ for higher Q (like changes of skewness or a non-monotonic change of the depth of consecutive troughs) indicate the possible presence of beats [58–60] in $S(Q)$ caused by Ni or Co addition which are discussed further in the Supplementary Material. Considering again the very similar X-ray form factors of Cu, Ni and Co as well as their virtually identical atomic diameters (Fig. 1) the differences in the $S(Q)$ point to differences in the structure of the three alloys which must be attributed to properties emerging from interactions between the added elements (Ni or Co) and the elements of the base ternary alloy (Zr, Cu, Al). To further elucidate the effect of the substitution of Cu by Ni or Co, $S(Q)$ for the ternary alloy was subtracted from those for the quaternary alloys and the so-obtained functions $\Delta S(Q)$ are plotted in Fig. 5b. Differences can be observed over the complete Q-range, highlighting the structural changes that arise from the atomic substitution.

Fig. 6a shows the reduced pair-distribution functions $G(r)$ for the three alloys obtained by Fourier-transforming the respective $S(Q)$ up to $Q_{max} = 25$ Å^{-1} (Eq. (1)). Again, a similar overall behaviour of the three alloys is visible with distinct broad peaks corresponding to the NN shells.

Following the shell/anti-shell concept introduced in Section 2.2 the r-ranges of the shells ($G(r) > 0$) are shaded and marked with dashed vertical lines in Fig. 6. Although these ranges can be considered equal for the three alloys, a general overall trend can be clearly observed: Ni or Co addition leads to a decrease of the amplitude of $G(r)$ for the NN shells accompanied by an increase of $G(r)$ within the anti-shells, effectively reducing deviations from the average density and thus indicating a more disordered structure.

The most obvious differences between the $G(r)$ for the three alloys (Fig. 6a) are in the first two NN shells. All three alloys show a split first NN shell similar to what has been previously observed in some Zr-based metallic glasses [30,32,61–63]. The split increases from a shoulder in the ternary alloy via a saddle point in the Ni-bearing to a minimum in the Co-bearing alloy.

The second $G(r)$ peak, corresponding to the second NN shell, is asymmetric and possesses shoulders at the low- as well as the high-r side. Especially the shoulder at about 5.9 Å weakens upon alloying. While the peak associated with the third NN shell is also asymmetric with a slight skewness towards higher r, all peaks related to higher NN shells are virtually symmetric, almost independent of the particular alloy, and $G(r)$ resembles a damped sinusoidal oscillation in this r-region. Underlying reasons for the possible existence of two regions with different order mechanisms (i.e. NN shells 1,2,3 compared to NN shells 4 and above) are discussed in the Supplementary Material in relation to local and global electronic interactions [27–29].

For further clarification, $\Delta G(r)$ functions corresponding to the difference between the $G(r)$ of the quaternary alloys and that of the ternary base alloy were calculated (Fig. 6b). The negative values of $\Delta G(r)$ clearly indicate that the amplitude of $G(r)$ within the regions of the NN shells decreases for the Ni- and Co-bearing alloys, whereas positive values of $\Delta G(r)$ occur mainly in the anti-shell regions corresponding to the increase of the $G(r)$ there. This corroborates the observation of a redistribution of atoms from the shells to the anti-shells reducing deviations from the average density, which can be interpreted as an increase of disorder in the short-to-medium-range order due to Ni or Co addition. The effect seems to be slightly bigger for the Co- than for the Ni-bearing alloy.

4. Discussion

The results in reciprocal (Fig. 5) as well as in real space (Fig. 6) suggest a small but unambiguous difference in the atomic structure of $Zr_{60}Cu_{30}Al_{10}$ following the addition of Ni or Co consistent with an increase in structural disorder. This direct comparison of different alloys is possible only because of the similar properties of Cu, Ni and Co, especially their initially almost identical sizes (Fig. 1). Keeping this in mind, a partial substitution of Cu by Ni or Co should not have any effect apart from Inoue's first empirical rule. However, a simple increase in the number of components cannot be effective towards an increase of disorder or GFA as long as the components are not associated with an increased diversity in their physical properties.

For a more detailed discussion in the present case it is instructive to start with a consideration of the first NN shell. The increase of its characteristic split as well as its width at the base (i.e. at $G(r) = 0$) compared to $Zr_{60}Cu_{30}Al_{10}$ (left inset of Fig. 6a and Fig. 7) is mainly due to a shift of the low-r portion towards lower r. From the Faber-Ziman

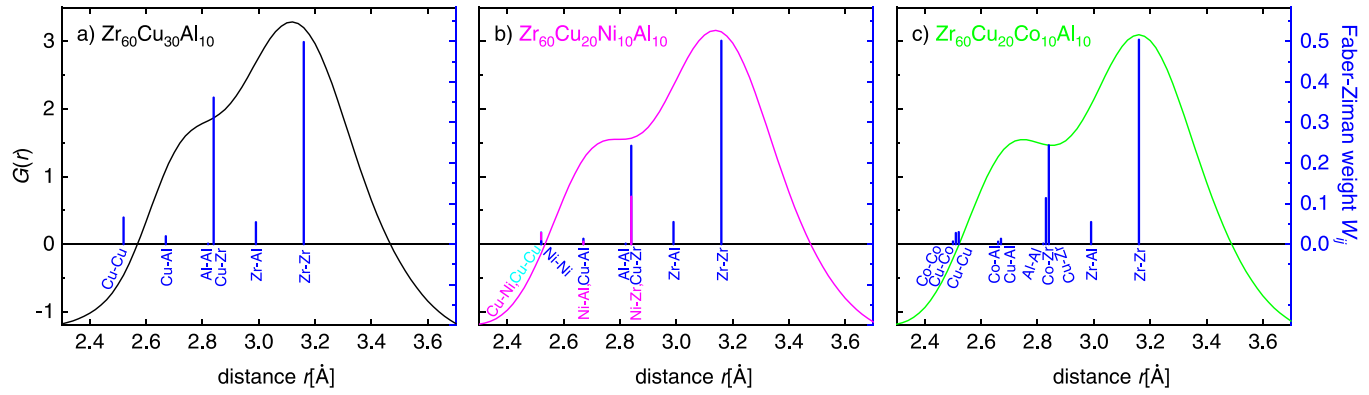

Fig. 7. $G(r)$ of the first NN shell for the three alloys together with the Faber-Ziman weighting factors W_{ij} (right y-axis) for the individual elemental pairs (blue bars; in case of pairs located at the same distance magenta or cyan bars in front of blue bars; the numerical values of W_{ij} can be found in Table S1 in the Supplementary Material) calculated using Eq. (2) and positioned at the interatomic distances d_{at} according to Fig. 1 (Table S1).

weighting factors [64]

$$W_{ij} = (2 - \delta_{ij}) \frac{c_i c_j f_i f_j}{\left(\sum_i c_i f_i\right)^2} \tag{2}$$

of the elemental pairs ij that are visualised as vertical bars (placed at interatomic distances from Fig. 1, height proportional to W_{ij}) in Fig. 7, as well as the probability [65,66]

$$P_{ij} = (2 - \delta_{ij}) c_i c_j = W_{ij} \frac{\left(\sum_i c_i f_i\right)^2}{f_i f_j} \tag{3}$$

of occurrence of these pairs, it can be assumed that the low-r feature is dominated by Cu-Zr as well as additional Ni-Zr or Co-Zr elemental pairs for the quaternary alloys (c_i, c_j are the atomic concentrations of the elements i and j, f_i, f_j their atomic form-factors neglecting the Q-dependence and δ_{ij} the Kronecker delta; the numerical values of W_{ij} and P_{ij} can be found in Table S1 in the Supplementary Material). The shift of the low-r feature towards lower r therefore suggests a shortening of the Ni-Zr and Co-Zr distances compared to those expected from Fig. 1, an effect that can be connected to the high negative ΔH_{mix} of Ni-Zr and Co-Zr compared to that of Cu-Zr (Fig. 1) [20,30,62,67]. Further differences between Cu and Ni or Co relate to details of the interatomic potentials associated with different bonding behaviour due to the different electronic configurations of Cu, Ni and Co. Bonding in the alloys with Ni or Co is expected to be more directional due to the participation of anisotropic d-states as opposed to the isotropic s-dominated bonding with Cu [68]. Hence, it is assumed that electronic interactions effectively change the initially almost identical sizes of Cu, Ni and Co, leading to an increase of the diversity in this property. Since this change cannot take place in these elements alone but becomes manifested only due to interactions with the other species (most importantly Zr) in the alloys, this can be considered as *emergent diversity* (in effective atomic sizes). Inoue's third rule [8] is utilised to increase confusion according to the second (and effectively also the first) route to enhance confusion and consequently GFA. Indeed, for the case of the two quaternary alloys studied here, $Zr_{60}Cu_{20}Ni_{10}Al_{10}$ and $Zr_{60}Cu_{20}Co_{10}Al_{10}$, the addition of Ni or Co to the ternary system $Zr_{60}Cu_{30}Al_{10}$, was found to improve GFA. While the critical diameter for the ternary alloys is 8 mm as reported by Zhang et al. [69], for the Ni-bearing quaternary $Zr_{60}Cu_{20}Ni_{10}Al_{10}$ it increases to 20 mm as reported by Son et al. [37]. For the Co-bearing alloy, $Zr_{60}Cu_{20}Co_{10}Al_{10}$, it could be confirmed in this study that $d_c \geq 10$ mm.

Extending the discussion to substitution-induced changes in the second NN shell shows most prominently a reduction of the shoulder on the high-r side of the according peak (Fig. 6a). Computer simulations related distances in the second NN shell to the interconnection of coordination polyhedra sharing different numbers of atoms [70,71]. According to these simulations, atoms in the second NN shell can be found at distances $2r_1$, $\sqrt{3}r_1$, $\sqrt{\frac{8}{3}}r_1$ or $\sqrt{2}r_1$ if their coordination polyhedra share 1, 2, 3 or 4 atoms with coordination polyhedra of atoms located at $r = 0$ Å, respectively, where r_1 is the position of the centroid of the first peak in $G(r)$. These characteristic distances are marked with vertical lines in the inset for the second NN shell in Fig. 6a. Accordingly, the observed changes in the present case point foremostly to a reduction in 1-atom interconnections which are not compensated by an increase in other interconnection schemes. Instead, it seems that the reduction is accompanied by an increase in the number of atoms in the adjacent anti-shell (inset of Fig. 6a). Thus, the observed changes for the second NN shell again corroborate the disordering induced by Ni or Co addition, with Co having the bigger effect.

Although every atom in the alloy is at the centre of "its own SRO" and the described local effects should therefore be reflected in the high-r region of $G(r)$ as well, its many-body nature may lead to additional emergent effects [51,72–74]. The local effects can be regarded to average out for higher distances, and are replaced by a coarse-grained description of the structure [51,73]. In the same manner, local electronic effects may become replaced by global electronic interactions [27,28,75]. Shells 4 and above show a common pattern in $\Delta G(r)$, i.e. an almost symmetrical redistribution of pair density to lower as well as higher r, with $\Delta G(r) < 0$ exclusively within the shells and $\Delta G(r) > 0$ exclusively for the anti-shell regions (Fig. 6b). To gain more insight into this behaviour, Fig. 9 shows the absolute values of the reduced pair distribution functions $|G(r)|$ for all three alloys in a semi-logarithmic plot highlighting the nearly exponential decay of the density oscillations with increasing distance r. This decay can be characterised by a structural coherence length ξ_s according to $G(r) \propto \exp(-/\xi_s)$ [51]. Overall, the addition of Ni or Co leads to a slight reduction of ξ_s (cf. straight lines in Fig. 9). In the Supplementary Material (Fig. S2), it is demonstrated that two $G(r)$, differing slightly only in their coherence lengths, lead to a $\Delta G(r)$ very similar to that observed in Fig. 6b for NN shells 4 and beyond. This suggests that disorder in the form of a reduced deviation from the average particle density is equivalent to a reduction in long-range density correlations, i.e. the redistribution of atoms from the shells to the anti-shells is reflected in a reduced coherence length ξ_s. Recently it was shown that ξ_s is nearly proportional to the height of the first peak in the structure factor $S(Q_1)$ of many metallic glass-forming alloys [76], which is in accordance with the alloying-induced reduction in $S(Q_1)$ observed in the present case (left inset of Fig. 5a).

Fig. 8 shows the DSC traces for the temperature ranges relevant to obtain the characteristic parameters reduced glass-transition temperature $T_{rg} = T_g/T_l$ and undercooled liquid region $\Delta T_X = T_X - T_g$ for the three alloys. The values are listed in Table 1 and are in agreement with data available in the literature [32,37,69,77,78]. T_g is practically the same for all three alloys. However, the addition of Ni increases T_X (thus

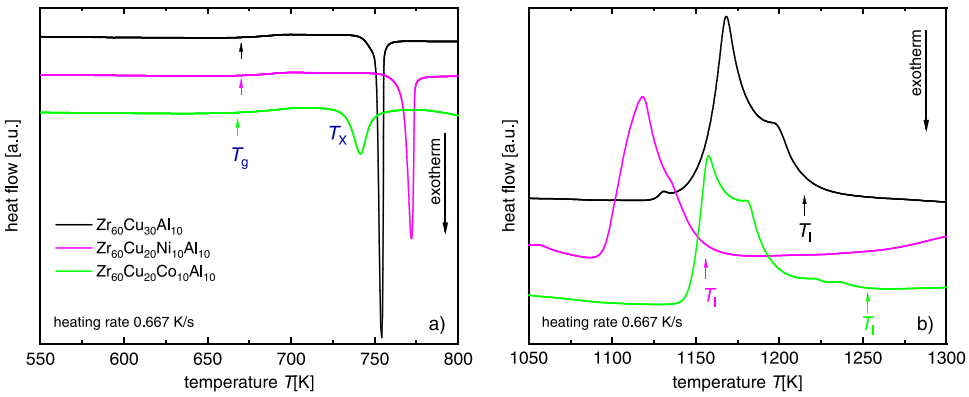

Fig. 8. DSC traces for the three alloys. The arrows indicate in a) the glass-transition temperature T_g and the onset crystallisation temperature T_X and in b) the liquidus temperature T_l. The curves are shifted along the *y*-axis for clarity.

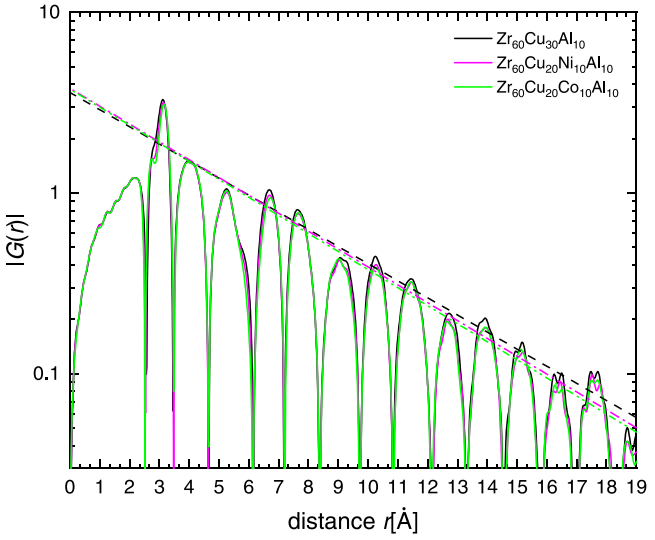

Fig. 9. The absolute values of the reduced pair distribution functions for all three alloys in a semi-logarithmic plot. The straight lines are linear guides for the eye. Their slopes correspond to the structural coherence lengths ξ_s.

Table 1
Glass−transition temperatures T_g, onset crystallisation temperatures TX and liquidus temperatures T_l as well as the reduced glass−transition temperatures $T_{rg} = T_g/T_l$ and the undercooled liquid regions $\Delta T_X = T_X - T_g$ for the alloys under consideration.

alloy	T_g [K]	T_X [K]	T_l [K]	T_{rg}	ΔT_X [K]
$Zr_{60}Cu_{30}Al_{10}$	670	751	1215	0.55	81
$Zr_{60}Cu_{20}Ni_{10}Al_{10}$	670	768	1156	0.58	98
$Zr_{60}Cu_{20}Co_{10}Al_{10}$	668	734	1253	0.53	66

increasing the thermal stability of the glassy phase) and reduces T_l, shifting T_{rg} closer to 2/3, the value considered optimal [14]. On the other hand, the glassy phase of the Co-bearing alloy exhibits lower T_X and lower T_{rg}. This indicates that the relationship between disorder and thermal stability of the glass phase is not monotonic.

In a future, more detailed study, calculations within the framework of density-functional theory (DFT), complementing those recently performed for the ternary alloy [32], could provide a better understanding of the alloying-induced changes to the local electronic interactions that lead to the observed structural changes and their effect on the thermal stability of the glass.

5. Conclusions

Insights into the effect of the addition of Ni or Co on the atomic structure of $Zr_{60}Cu_{30}Al_{10}$ bulk metallic glass were gained using high-energy synchrotron radiation X-ray diffraction. The additions cause an increase of disorder of the amorphous structure. This becomes manifest in the short- and medium-range order by an overall decrease in the amplitude of the oscillations in the reduced pair-distribution function $G(r)$ and the reduction of the structural coherence length ξ_s. Both are related to a redistribution of atoms from the nearest-neighbour shells towards the anti-shells. The novel concept of anti-shells introduced here provides a fruitful basis to facilitate the description of disordering in amorphous alloys. Disorder is connected to increased confusion resulting from an increased diversity of atomic species and their different sizes under introduction of a further component. Electronic interactions can cause an increase of diversity of atomic sizes leading to an emergent increase of confusion. Adding further elements might at the same time impact other factors, leading to an overall decrease of the thermal stability of the glassy phase. Increasing structural disorder does not necessarily imply increasing stability. Nevertheless, further routes to "confusion enhancement" need to be explored, and more quantitative measures of confusion are sought.

CRediT authorship contribution statement

Martin E. Stiehler: Conceptualisation, Methodology, Writing – original draft, Data curation, Visualisation. **Nikolaos T. Panagiotopoulos:** Investigation, Writing – original draft, Visualisation. **Dean S. Keeble:** Investigation, Formal analysis, Writing – review & editing. **Yurii P. Ivanov:** Investigation, Writing – review & editing, Formal analysis, Visualisation. **Melita Menelaou:** Writing – review & editing. **Mark R. Jolly:** Supervision, Writing – review & editing, Funding acquisition. **A. Lindsay Greer:** Formal analysis, Writing – review & editing, Funding acquisition. **Konstantinos Georgarakis:** Conceptualisation, Methodology, Writing – original draft, Project administration, Supervision, Funding acquisition.

Declaration of Competing Interest

The authors declare that they have no known competing financial interests or personal relationships that could have appeared to influence the work reported in this paper.

Data Availability

The raw/processed data required to reproduce the findings of this study are available from the corresponding author upon reasonable request.

Acknowledgements

Experimental support by the Diamond Light Source, UK, under the Rapid Access scheme at beamline I15–1 (CY22841: "Uncovering structural features of Zr-Cu-Al-based BMGs") as well as financial support from the EPSRC-DTP project "Bulk Metallic Glasses: Revealing the Structural Pathway of Liquid Metals to Vitrification" (ref. 2043971) in the framework of the EPSRC (Engineering and Physical Sciences Research Council, UK) Doctoral Training Partnership (DTP) with Cranfield University (EP/N509450/1) and the ERC (European Research Council, EU) project "Extending the range of the glassy state: Exploring structure and property limits in metallic glasses" (grant agreement ID: 695487) is gratefully acknowledged. The authors thank Zhi Wang for fruitful discussions and Steve Pope for his support in sample preparation.

Appendix A. Supporting information

Supplementary data associated with this article can be found in the online version at doi:10.1016/j.mtcomm.2022.103531.

References

[1] M.M. Khan, A. Nemati, Z.U. Rahman, U.H. Shah, H. Asgar, W. Haider, Recent advancements in bulk metallic glasses and their applications: a review, Crit. Rev. Solid State 43 (2018) 233, https://doi.org/10.1080/10408436.2017.1358149.
[2] A.L. Greer, Metallic glasses…on the threshold, Mater. Today 12 (2009) 14, https://doi.org/10.1016/S1369-7021(09)70037-9.
[3] M.A. Yousfi, N.T. Panagiotopoulos, A.M. Jorge Junior, K. Georgarakis, A.R. Yavari, Novel micro-flat springs using the superior elastic properties of metallic glass foils, Scr. Mater. 131 (2017) 84, https://doi.org/10.1016/j.scriptamat.2017.01.012.
[4] Y. Sun, A. Concustell, A.L. Greer, Thermomechanical processing of metallic glasses: Extending the range of the glassy state, Nat. Rev. Mater. 1 (2016) 16039, https://doi.org/10.1038/natrevmats.2016.39.
[5] N.T. Panagiotopoulos, K. Georgarakis, A.M. Jorge Jr, M. Aljerf, W.J. Botta, A. L. Greer, A.R. Yavari, Advanced ultra-light multifunctional metallic-glass wave springs, Mater. Des. 192 (2020), 108770, https://doi.org/10.1016/j.matdes.2020.108770.
[6] A.L. Greer, Confusion by design, Nature 366 (1993) 303, https://doi.org/10.1038/366303a0.
[7] A.L. Greer, Metallic glasses, Science 267 (1995) 1947, https://doi.org/10.1126/science.267.5206.1947.
[8] A. Inoue, Stabilization of metallic supercooled liquid and bulk amorphous alloys, Acta Mater. 48 (2000) 279, https://doi.org/10.1016/S1359-6454(99)00300-6.
[9] S. Ganorkar, S. Lee, Y.H. Lee, T. Ishikawa, G.W. Lee, Origin of glass forming ability of Cu-Zr alloys: A link between compositional variation and stability of liquid and glass, Phys. Rev. Mater. 2 (2018) 1, https://doi.org/10.1103/PhysRevMaterials.2.115606.
[10] J. Russo, F. Romano, H. Tanaka, Glass forming ability in systems with competing orderings, Phys. Rev. X 8 (2018) 21040, https://doi.org/10.1103/PhysRevX.8.021040.
[11] K.F. Kelton, A.L. Greer, D.M. Herlach, D. Holland-Moritz, The influence of order on the nucleation barrier, MRS Bull. 29 (2004) 940, https://doi.org/10.1557/mrs2004.264.
[12] D. Turnbull, Amorphous solid formation and interstitial solution behavior in metallic alloy systems, J. Phys. Colloq. 35 (1974) C4, https://doi.org/10.1051/jphyscol:1974401.
[13] A.L. Greer, N. Karpe, J. Bøttiger, Diffusional aspects of the solid state amorphization reaction, J. Alloy. Compd. 194 (1993) 199, https://doi.org/10.1016/0925-8388(93)90003-6.
[14] D. Turnbull, Under what conditions can a glass be formed? Contemp. Phys. 10 (1969) 473, https://doi.org/10.1080/00107516908204405.
[15] M.H. Bhat, V. Molinero, E. Soignard, V.C. Solomon, S. Sastry, J.L. Yarger, C. A. Angell, Vitrification of a monatomic metallic liquid, Nature 448 (2007) 787, https://doi.org/10.1038/nature06044.
[16] A.R. Yavari, Solving the puzzle of eutectic compositions with "Miracle glasses", Nat. Mater. 4 (2005) 2, https://doi.org/10.1038/nmat1289.
[17] E. Perim, D. Lee, Y. Liu, C. Toher, P. Gong, Y. Li, W.N. Simmons, O. Levy, J. J. Vlassak, J. Schroers, S. Curtarolo, Spectral descriptors for bulk metallic glasses based on the thermodynamics of competing crystalline phases, Nat. Commun. 7 (2016) 12315, https://doi.org/10.1038/ncomms12315.
[18] K. Georgarakis, A.R. Yavari, D.V. Louzguine-Luzgin, G. Vaughan, Crystallization and vitrification of a PdCuNiP metallic glass upon thermal and mechanical processes detected by synchrotron light X-ray radiation, AIP Conf. Proc. (2013) 672–681, https://doi.org/10.1063/1.4794657.
[19] R. Dai, R. Ashcraft, A.K. Gangopadhyay, K.F. Kelton, Predicting metallic glass formation from properties of the high temperature liquid, J. Non Cryst. Solids 525 (2019), 119673, https://doi.org/10.1016/j.jnoncrysol.2019.119673.
[20] I. Kaban, P. Jóvári, V. Kokotin, O. Shuleshova, B. Beuneu, K. Saksl, N. Mattern, J. Eckert, A.L. Greer, Local atomic arrangements and their topology in Ni-Zr and Cu-Zr glassy and crystalline alloys, Acta Mater. 61 (2013) 2509, https://doi.org/10.1016/j.actamat.2013.01.027.
[21] M.-B. Tang, D.-Q. Zhao, M.-X. Pan, W.-H. Wang, Binary Cu-Zr bulk metallic glasses, Chin. Phys. Lett. 21 (2004) 901, https://doi.org/10.1088/0256-307X/21/5/039.
[22] L. Xia, W.H. Li, S.S. Fang, B.C. Wei, Y.D. Dong, Binary Ni-Nb bulk metallic glasses, J. Appl. Phys. 99 (2006), 026103, https://doi.org/10.1063/1.2158130.
[23] T. Egami, M. Ojha, D.M. Nicholson, D.V. Louzguine-Luzgin, N. Chen, A. Inoue, Glass formability and the Al-Au system, Philos. Mag. 92 (2012) 655, https://doi.org/10.1080/14786435.2011.630692.
[24] Y. Wang, J. Yao, Y. Li, Glass formation adjacent to the intermetallic compounds in Cu-Zr binary system, J. Mater. Sci. Technol. 34 (2018) 605, https://doi.org/10.1016/j.jmst.2017.09.008.
[25] D. Wang, Y. Li, B.B. Sun, M.L. Sui, K. Lu, E. Ma, Bulk metallic glass formation in the binary Cu-Zr system, Appl. Phys. Lett. 84 (2004) 4029, https://doi.org/10.1063/1.1751219.
[26] C.E. Lekka, G.A. Evangelakis, Bonding characteristics and strengthening of CuZr fundamental clusters upon small Al additions from density functional theory calculations, Scr. Mater. 61 (2009) 974, https://doi.org/10.1016/j.scriptamat.2009.08.008.
[27] P. Häussler, Interrelations between atomic and electronic structures - Liquid and amorphous metals as model systems, Phys. Rep. 222 (1992) 65, https://doi.org/10.1016/0370-1573(92)90018-U.
[28] M.E. Stiehler, M.R. Jolly, K. Georgarakis, On the impact of global interactions on the structure of metallic glasses, J. Alloy. Compd. 782 (2019) 496, https://doi.org/10.1016/j.jallcom.2018.12.086.
[29] C.C. Yuan, F. Yang, X.K. Xi, C.L. Shi, D. Holland-Moritz, M.Z. Li, F. Hu, B.L. Shen, X. L. Wang, A. Meyer, W.H. Wang, Impact of hybridization on metallic-glass formation and design, Mater. Today 32 (2020) 26, https://doi.org/10.1016/j.mattod.2019.06.001.
[30] K. Georgarakis, A.R. Yavari, D.V. Louzguine-Luzgin, J. Antonowicz, M. Stoica, Y. Li, M. Satta, A. LeMoulec, G. Vaughan, A. Inoue, Atomic structure of Zr-Cu glassy alloys and detection of deviations from ideal solution behavior with Al addition by x-ray diffraction using synchrotron light in transmission, Appl. Phys. Lett. 94 (2009) 48, https://doi.org/10.1063/1.3136428.
[31] J. Antonowicz, A. Pietnoczka, W. Zalewski, R. Bacewicz, M. Stoica, K. Georgarakis, A.R. Yavari, Local atomic structure of Zr-Cu and Zr-Cu-Al amorphous alloys investigated by EXAFS method, J. Alloy. Compd. 509 (2011) S34, https://doi.org/10.1016/j.jallcom.2010.10.105.
[32] K. Georgarakis, L. Hennet, G.A. Evangelakis, J. Antonowicz, G.B. Bokas, V. Honkimaki, A. Bytchkov, M.W. Chen, A.R. Yavari, Probing the structure of a liquid metal during vitrification, Acta Mater. 87 (2015) 174, https://doi.org/10.1016/j.actamat.2015.01.005.
[33] N. Mattern, A. Schöps, U. Kühn, J. Acker, O. Khvostikova, J. Eckert, Structural behavior of Cu_xZr_{100-x} metallic glass (x=35-70), J. Non Cryst. Solids 354 (2008) 1054, https://doi.org/10.1016/j.jnoncrysol.2007.08.035.
[34] Y.Q. Cheng, E. Ma, H.W. Sheng, Atomic level structure in multicomponent bulk metallic glass, Phys. Rev. Lett. 102 (2009) 1, https://doi.org/10.1103/PhysRevLett.102.245501.
[35] A. Takeuchi, A. Inoue, Classification of bulk metallic glasses by atomic size difference, heat of mixing and period of constituent elements and its application to characterization of the main alloying element, Mater. Trans. JIM 46 (2005) 2817, https://doi.org/10.2320/matertrans.46.2817.
[36] D.B. Miracle, D.V. Louzguine-Luzgin, L.V. Louzguina-Luzgina, A. Inoue, An assessment of binary metallic glasses: correlations between structure, glass forming ability and stability, Int. Mater. Rev. 55 (2010) 218, https://doi.org/10.1179/095066010×12646898728200.
[37] K.S. Son, X.M. Wang, Y. Yokoyama, K. Yubuta, A. Inoue, Formation, thermal stability, and mechanical properties of glassy $Zr_{60}Al_{10}Ni_{10}Cu_{20}$ alloy rods with diameters of 18 and 20 mm, Mater. Trans. 50 (2009) 2021, https://doi.org/10.2320/matertrans.MRA2008419.
[38] A. Inoue, T. Zhang, Fabrication of bulk glassy $Zr_{55}Al_{10}Ni_5Cu_{30}$ alloy of 30 mm in diameter by a suction casting method, Mater. Trans. JIM 37 (1996) 185, https://doi.org/10.2320/matertrans1989.37.185.
[39] Y. Yokoyama, E. Mund, A. Inoue, L. Schultz, Production of $Zr_{55}Cu_{30}Ni_5Al_{10}$ glassy alloy rod of 30 mm in diameter by a cap-cast technique, Mater. Trans. JIM 48 (2007) 3190, https://doi.org/10.2320/matertrans.MRP2007164.
[40] K. Han, J. Qiang, Y. Wang, B. Zhao, P. Häussler, $Zr_{55.8}Al_{19.4}(Co_{1-x}Cu_x)_{24.8}$ (x=0-0.8 at%) bulk metallic glasses for surgical devices applications, J. Iron Steel Res. Int. 25 (2018) 644, https://doi.org/10.1007/s42243-018-0085-4.
[41] D.B. Miracle, A structural model for metallic glasses, Nat. Mater. 3 (2004) 697, https://doi.org/10.1038/nmat1219.
[42] M. Basham, J. Filik, M.T. Wharmby, P.C.Y. Chang, B. El Kassaby, M. Gerring, J. Aishima, K. Levik, B.C.A. Pulford, I. Sikharulidze, D. Sneddon, M. Webber, S. S. Dhesi, F. Maccherozzi, O. Svensson, S. Brockhauser, G. Náray, A.W. Ashton, Data Analysis WorkbeNch (DAWN), J. Synchrotron Radiat. 22 (2015) 853, https://doi.org/10.1107/S1600577515002283.
[43] J. Filik, A.W. Ashton, P.C.Y. Chang, P.A. Chater, S.J. Day, M. Drakopoulos, M. W. Gerring, M.L. Hart, O.V. Magdysyuk, S. Michalik, A. Smith, C.C. Tang, N. J. Terrill, M.T. Wharmby, H. Wilhelm, Processing two-dimensional X-ray diffraction and small-angle scattering data in DAWN 2, J. Appl. Crystallogr. 50 (2017) 959, https://doi.org/10.1107/S1600576717004708.
[44] A.K. Soper, GudrunN and GudrunX: Programs for correcting raw neutron and X-ray diffraction data to differential scattering cross section. Rutherford Appleton Laboratory Technical Report RAL-TR-2011–013, Science and Technology Facilities Council, Didcot, 2011. ⟨https://www.worldcat.org/title/gudrunn-and-gudrunx

-programs-for-correcting-raw-neutron-and-x-ray-diffraction-data-to-differential-scattering-cross-section/oclc/747917333) (Accessed 10 April 2019).
[45] J. Krogh-Moe, A method for converting experimental X-ray intensities to an absolute scale, Acta Crystallogr. 9 (1956) 951, https://doi.org/10.1107/S0365110×56002655.
[46] N. Norman, The Fourier transform method for normalizing intensities, Acta Crystallogr. 10 (1957) 370, https://doi.org/10.1107/S0365110×57001085.
[47] T. Egami, S.J.L. Billinge, Underneath the Bragg Peaks: Structural Analysis of Complex Materials, Pergamon Press Ltd, 2003.
[48] Y. Waseda, The Structure of Non-Crystalline Materials: Liquids and Amorphous Solids, McGraw-Hill, 1980.
[49] Z. Wang, S.V. Ketov, C.L. Chen, Y. Shen, Y. Ikuhara, A.A. Tsarkov, D.V. Louzguine-Luzgin, J.H. Perepezko, Nucleation and thermal stability of an icosahedral nanophase during the early crystallization stage in Zr-Co-Cu-Al metallic glasses, Acta Mater. 132 (2017) 298, https://doi.org/10.1016/j.actamat.2017.04.044.
[50] G.S. Cargill, Structure of metallic alloy glasses, in: H. Ehrenreich, F. Seitz, D. Turnbull (Eds.), Solid State Physics. Advances in Research and Applications, Academic Press, 1975, pp. 227–320, https://doi.org/10.1016/S0081-1947(08)60337-9.
[51] C.W. Ryu, W. Dmowski, T. Egami, Ideality of liquid structure: a case study for metallic alloy liquids, Phys. Rev. E 101 (2020), 030601, https://doi.org/10.1103/PhysRevE.101.030601.
[52] Y.Q. Cheng, E. Ma, Atomic-level structure and structure-property relationship in metallic glasses, Prog. Mater. Sci. 56 (2011) 379, https://doi.org/10.1016/j.pmatsci.2010.12.002.
[53] H. Tanaka, Roles of local icosahedral chemical ordering in glass and quasicrystal formation in metallic glass formers, J. Phys. Condens. Matter 15 (2003) L491, https://doi.org/10.1088/0953-8984/15/31/102.
[54] S. Sachdev, D.R. Nelson, Theory of the structure factor of metallic glasses, Phys. Rev. Lett. 53 (1984) 1947, https://doi.org/10.1103/PhysRevLett.53.1947.
[55] K.F. Kelton, G.W. Lee, A.K. Gangopadhyay, R.W. Hyers, T.J. Rathz, J.R. Rogers, M. B. Robinson, D.S. Robinson, First X-ray scattering studies on electrostatically levitated metallic liquids: demonstrated influence of local icosahedral order on the nucleation barrier, Phys. Rev. Lett. 90 (2003), 195504, https://doi.org/10.1103/PhysRevLett.90.195504.
[56] E. Ma, Tuning order in disorder, Nat. Mater. 14 (2015) 547, https://doi.org/10.1038/nmat4300.
[57] R. Dai, R. Ashcraft, K.F. Kelton, A possible structural signature of the onset of cooperativity in metallic liquids, J. Chem. Phys. 148 (2018), 204502, https://doi.org/10.1063/1.5026801.
[58] F.S. Crawford Jr., Waves (Berkeley Physics Course, Volume 3), McGraw-Hill College, 1968.
[59] J. Blétry, Geometrical models for liquid metals and alloys, Z. Naturforsch. A 33 (1978) 327, https://doi.org/10.1515/zna-1978-0311.
[60] E. Zaccarelli, G. Foffi, K.A. Dawson, S.V. Buldyrev, F. Sciortino, P. Tartaglia, Static and dynamical correlation functions behaviour in attractive colloidal systems from theory and simulation, J. Phys. Condens. Matter 15 (2003) S367, https://doi.org/10.1088/0953-8984/15/1/350.
[61] M. Steyer, H.-U. Krebs, H.C. Freyhardt, Short-range order in metallic Co-Zr glasses, Z. Phys. B 66 (1987) 317, https://doi.org/10.1007/BF01305421.
[62] K. Georgarakis, A.R. Yavari, M. Aljerf, D.V. Louzguine-Luzgin, M. Stoica, G. Vaughan, A. Inoue, On the atomic structure of Zr-Ni and Zr-Ni-Al metallic glasses, J. Appl. Phys. 108 (2010) 1, https://doi.org/10.1063/1.3446131.
[63] N. Hua, S. Pang, Y. Li, J. Wang, R. Li, K. Georgarakis, A.R. Yavari, G. Vaughan, T. Zhang, Ni- and Cu-free Zr-Al-Co-Ag bulk metallic glasses with superior glass-forming ability, J. Mater. Res. 26 (2011) 539, https://doi.org/10.1557/jmr.2010.65.
[64] T.E. Faber, J.M. Ziman, A theory of the electrical properties of liquid metals III, The resistivity of binary alloys, Philos. Mag. 11 (1965) 153, https://doi.org/10.1080/14786436508211931.
[65] C. Jelsch, K. Ejsmont, L. Huder, The enrichment ratio of atomic contacts in crystals, an indicator derived from the Hirshfeld surface analysis, IUCrJ 1 (2014) 119, https://doi.org/10.1107/S2052252514003327.
[66] X. Tong, G. Wang, Z.H. Stachurski, J. Bednarčík, N. Mattern, Q.J. Zhai, J. Eckert, Structural evolution and strength change of a metallic glass at different temperatures, Sci. Rep. 6 (2016) 30876, https://doi.org/10.1038/srep30876.
[67] J. Antonowicz, D.V. Louzguine-Luzgin, A.R. Yavari, K. Georgarakis, M. Stoica, G. Vaughan, E. Matsubara, A. Inoue, Atomic structure of Zr-Cu-Al and Zr-Ni-Al amorphous alloys, J. Alloy. Compd. 471 (2009) 70, https://doi.org/10.1016/j.jallcom.2008.03.092.
[68] Z. Wang, F. Yang, A. Bernasconi, K. Samwer, A. Meyer, Predicting structural and dynamical behavior of La-based glasses and melts from the anharmonicity in their interatomic potential, Phys. Rev. B 98 (2018) 1, https://doi.org/10.1103/PhysRevB.98.024204.
[69] Q.S. Zhang, W. Zhang, D.V. Louzguine-Luzgin, A. Inoue, High glass-forming ability and unusual deformation behavior of new Zr-Cu-Fe-Al bulk metallic glasses, Mater. Sci. Forum 654–656 (2010) 1042, https://doi.org/10.4028/www.scientific.net/MSF.654-656.1042.
[70] C.H. Bennett, Serially deposited amorphous aggregates of hard spheres, J. Appl. Phys. 43 (1972) 2727, https://doi.org/10.1063/1.1661585.
[71] J. Ding, E. Ma, M. Asta, R.O. Ritchie, Second-nearest-neighbor correlations from connection of atomic packing motifs in metallic glasses and liquids, Sci. Rep. 5 (2015) 1, https://doi.org/10.1038/srep17429.
[72] T. Egami, Local density correlations in liquids, Front. Phys. 8 (2020) 1, https://doi.org/10.3389/fphy.2020.00050.
[73] C.W. Ryu, T. Egami, Medium-range atomic correlation in simple liquids. I. Distinction from short-range order, Phys. Rev. E 104 (2021), 064109, https://doi.org/10.1103/PhysRevE.104.064109.
[74] P.W. Anderson, More is different, Science 177 (1972) 393, https://doi.org/10.1126/science.177.4047.393.
[75] P. Häussler, J. Barzola-Quiquia, D. Hauschild, J. Rauchhaupt, M. Stiehler, M. Hackert, Spherical periodicity, a general feature of matter at its early stages of formation, in: T.B. Massalski, P.E.A. Turchi (Eds.), TMS Annual Meeting, The Minerals, Metals and Materials Society, 2005, pp. 43–86.
[76] C.W. Ryu, W. Dmowski, K.F. Kelton, G.W. Lee, E.S. Park, J.R. Morris, T. Egami, Curie-Weiss behavior of liquid structure and ideal glass state, Sci. Rep. 9 (2019) 18579, https://doi.org/10.1038/s41598-019-54758-y.
[77] A. Inoue, T. Negishi, H.M. Kimura, T. Zhang, A.R. Yavari, High packing density of Zr- and Pd-based bulk amorphous alloys, Mater. Trans. JIM 39 (1998) 318, https://doi.org/10.2320/matertrans1989.39.318.
[78] S.V. Ketov, A.S. Trifonov, Y.P. Ivanov, A.Y. Churyumov, A.V. Lubenchenko, A. A. Batrakov, J. Jiang, D.V. Louzguine-Luzgin, J. Eckert, J. Orava, A.L. Greer, On cryothermal cycling as a method for inducing structural changes in metallic glasses, NPG Asia Mater. 10 (2018) 137, https://doi.org/10.1038/s41427-018-0019-4.